Applied Catalysis A: General 458 (2013) 63–70

Contents lists available at SciVerse ScienceDirect

Applied Catalysis A: General

journal homepage: www.elsevier.com/locate/apcata

Highly efficient and stable Au/Mn_2O_3 catalyst for oxidative cyclization of 1,4-butanediol to γ-butyrolactone

Xian Li[a], Yuanyuan Cui[a], Xinli Yang[b], Wei-Lin Dai[a,*], Kangnian Fan[a]

[a] Department of Chemistry and Shanghai Key Laboratory of Molecular Catalysis and Innovative Materials, Fudan University, Shanghai 200433, PR China
[b] College of Chemistry & Chemical Engineering, Henan University of Technology, Zhengzhou 450001, Henan, PR China

ARTICLE INFO

Article history:
Received 2 February 2013
Received in revised form 11 March 2013
Accepted 16 March 2013
Available online xxx

Keywords:
Au/Mn_2O_3 catalyst
Manganese oxides supports
1,4-Butanediol
Oxidative lactionzation

ABSTRACT

In this work, gold nanoparticles deposited on manganese sesquioxide (Mn_2O_3) showed high activity in the oxidative lactonization of 1,4-butanediol to γ-butyrolactone with air as the oxidant. On the contrary, nano-sized gold supported on manganese dioxide (MnO_2) and manganese oxide (MnO) presented much lower activities. XRD, TEM and XPS characterizations revealed that the superior catalytic performance of Au/Mn_2O_3 could be ascribed to the highest dispersion of gold particles and unique intrinsic properties of Mn_2O_3, which possesses the appropriate point of zero charge for deposition–precipitation method, the most quantity of oxygen vacancies and the appropriate gold–support interaction. Au/Mn_2O_3 exhibited selectivity of 100%, which could facilitate the purification of target product from the reaction mixture. Furthermore, the as-prepared Au/Mn_2O_3 catalyst could be recovered by simple filtration, and used repetitively or preserved for a long period without apparent loss of activity.

1. Introduction

The selective synthesis of lactones has attracted much interest to both academic and industrial chemists. Among the lactones, γ-butyrolactone is widely used as a significant solvent, extraction agent and intermediate in agriculture, petroleum industry, pharmaceutics and fibers [1–4]. Moreover, the aerobic oxidation of 1,4-butanediol to γ-butyrolactone is considered as one of the most promising pathway for industrially acceptable process, owing to the absence of waste or pollutant.

Traditionally, the lactonization of 1,4-butanediol was carried out in metal reagents [5,6]. Then several homogeneous [7,8] or heterogeneous catalysts [9,10] were used in the presence of organic co-oxidants such as ketones and alkenes, but these chemicals are expensive and/or toxic. Zhao and Hartwig reported that ruthenium complexes catalyzed this reaction with high activity and high turnover numbers even without solvents or hydrogen acceptors [11]. In recent years, supported gold catalysts, including gold deposited on hydrotalcite [12], gold particles supported on γ-AlOOH and γ-Al_2O_3 [13], and gold supported on anion-exchange resin Dowex Marathon MSA [14], have attracted tremendous attention to the synthesis of lactones from diols with admirable catalytic activities. Conventionally, support plays a crucial role in the performance of active gold catalysts apart from gold particle size [15,16], and reducible support is supposed to provide oxygen adsorption and activation sites, which can facilitate the oxidation process [16,17], thus it is believed that gold supported on reducible oxides are more active and stable than on inert oxides [17,18]. As expected, the outstanding catalytic performance for the oxidation of 1,4-butanediol to γ-butyrolactone has been obtained from finely dispersed Au on reducible oxides, such as TiO_2 [19], Fe_2O_3 [20,21], and Fe–Al–O composite [22].

Manganese oxides (MnO_x), as reducible oxides, have long been used as highly active, durable and low cost catalysts for aerobic oxidation of organic compounds [23–26]. For example, MnO_2 exhibited remarkably high catalytic activity and selectivity for the ammoxidation of alcohols [27]. When cooperated with gold nanoparticles, the catalytic activities were enhanced markedly for the oxidation of CO [28–31] or alcohols [27,32,33]. However, to the best of our knowledge, there has been no reports on the lactonization of 1,4-butanediol catalyzed by gold supported on manganese oxides. Herein, for the first time, we report the synthesis and catalytic application of Au nanoparticle catalysts supported on different manganese oxides in the oxidation of 1,4-butanediol to γ-butyrolactone with air as the sole oxidant. Additionally, the gold-supported catalysts are generally thought to be unstable and easy to deactivate, especially after a long period preservation or reused for many cycles because of the high activity of the nano-sized gold particles [34,35]. In this work, we also investigated the stability of the as-prepared Au/Mn_2O_3 catalyst.

* Corresponding author. Tel.: +86 21 55664678; fax: +86 21 55665701.
E-mail address: wldai@fudan.edu.cn (W.-L. Dai).

0926-860X/$ – see front matter © 2013 Elsevier B.V. All rights reserved.
http://dx.doi.org/10.1016/j.apcata.2013.03.020

2. Experimental

2.1. Catalyst preparation

Three kinds of different manganese oxides (MnO_2, Mn_2O_3 and MnO) were prepared according to the following preparation procedures as described elsewhere [25,26]. MnO_2 was prepared via hydrothermal method. Equal amount of $MnSO_4{\cdot}H_2O$ and $(NH_4)_2S_2O_8$ (both 50 ml, ca. 0.04 M) was mixed in a 250 ml round bottomed flask. The as-obtained mixture was hydrothermally processed at 393 K for 12 h, followed by filtration, washed with deionized water for 4 times and dried at 373 K for 12 h. Mn_2O_3 was obtained by calcination of $MnCO_3$ powder at 773 K for 4 h in static air and then cooled to room temperature. MnO was obtained by decomposition of $MnCO_3$ sample under pure N_2 atmosphere at 673 K for 4 h, and then cooled to room temperature in flowing N_2 stream.

Gold nanoparticles deposited on the as-synthesized manganese oxides with a nominal Au loading of 5 wt.% were carried out by deposition–precipitation (DP) method using urea as precipitation agent [36–38]. In a typical procedure, 15 ml of $HAuCl_4$ aqueous solution (2.43×10^{-3} M) was mixed with 60 ml of deionized water with continuous stirring, followed by the addition of 2.5 g of urea and 1.4 g of MnO_x. The mixture was heated to 363 K gradually and maintained for 4 h. After this step, the pH values of solutions were about 8.0, 8.0 and 8.5 for Au/MnO, Au/MnO_2 and Au/Mn_2O_3, respectively. The solid mass was filtered, washed with deionized water for 4 times, and dried in air overnight at 373 K. Finally, the Au/MnO_2 and Au/Mn_2O_3 samples were calcined at 573 K for 4 h in air, while the Au/MnO sample was calcined at 573 K for 4 h in flowing N_2 to avoid the oxidation of MnO by air.

2.2. Catalyst characterization

The specific surface area of samples was determined by nitrogen adsorption at 77 K (Micromeritics Tristar ASAP 3000) using the Brunauer–Emmett–Teller (BET) method. The gold loadings were determined by the inductively coupled plasma method (ICP, thermo E. IRIS). The XRD patterns were recorded on a Bruker D8 Advance diffractometer with Cu Kα radiation (λ = 0.154 nm), operated at 40 mA and 40 kV. The TEM micrographs were obtained on a JOEL JEM 2010 transmission electron microscope. The average size of the Au particles and relative distributions were estimated by counting more than 300 Au particles. The turnover frequency (TOF) was calculated by the amount of surface gold atoms and the mole diol reacted in the initial 2 h on per mole surface gold. The gold particles were assumed as sphere shape with a single gold atom diameter of 0.1442 nm. According to the gold atom diameter and the average gold particle size from TEM, the amount of surface gold atoms could be estimated, and the TOF value could be obtained [19–21]. The turnover number (TON) can also be obtained by the mole diol reacted per mole gold during the reaction. The XPS spectra were acquired under ultra high vacuum (<10^{-6} Pa) at a pass energy of 93.90 eV on a Perkin-Elmer PHI 5000C ESCA system equipped with a dual X-ray source using an Mg Kα (1253.6 eV) anode and a hemispheric energy analyzer. All binding energies were calibrated by using contaminant carbon (C 1s = 284.6 eV) as a reference.

2.3. Activity test

Catalyst tests were performed using a stainless steel autoclave equipped with a magnetic stirrer at 393 K. 1.4 g of 1,4-butanediol was dissolved in 20 ml of tributyl phosphate (TBP), followed by the addition of 0.3 g of Au/MnO_x catalyst. Then the autoclave was sealed and filled with 1.25 MPa air. The rate of magnetic stirring was set at 800 rpm simultaneously. The reaction mixture was sampled at regular time intervals and analyzed by gas chromatography (GC9560 (HuaAi Co. Ltd.) with a FID detector and HP5 capillary column) to determine the conversion and selectivity. Gas chromatography–mass spectrometry (GC 8000 TOF-MS voyager) was utilized to detect the product distribution.

Recycling experiments over Au/Mn_2O_3 catalyst were conducted under identical reaction conditions as the above. The used catalyst was collected by filtration, and recovered by being washed with ethanol 3 times and drying overnight at 373 K in air.

3. Results and discussion

3.1. Catalyst characterization

3.1.1. BET and ICP-AES

In Table 1, the data show that MnO_2 has the highest BET surface area (52 m^2/g), while Mn_2O_3 is 35 m^2/g and MnO is the lowest (10 m^2/g). Because Mn_2O_3 and MnO were prepared from the same precursor, the difference in BET values is attributed to the effect of different treating atmosphere. Support effect is always significant in gold catalysts, so we tried to synthesize manganese oxides with similar morphology for comparing the effect of the support crystal phase reasonably. After the deposition of gold, the BET surface area decreases moderately, and the values turn to 8.0, 39 and 31 m^2/g for Au/MnO, Au/MnO_2 and Au/Mn_2O_3 with no sharp changes for the used one. In addition, the real gold loadings of the three catalysts are all near the nominal amount (5%) as determined by ICP-AES method with the error range of ±0.5%.

3.1.2. XRD patterns

Fig. 1 shows XRD patterns of Au/MnO_x. It can be found that all of the supports are in pure crystal phases, and the addition of gold causes no structural changes for the support. In fresh (Fig. 1(a)) and used Au/Mn_2O_3 (Fig. 1(b)), the XRD patterns exhibit well-defined diffraction characteristics of Mn_2O_3 (JCPDS 41-1442), and there is no distinct gold reflection owing to the high dispersion of Au particles. For Au/MnO (Fig. 1(c)), the reflections are mainly attributed to MnO (JCPDS 06-0592) with a small amount of Mn_3O_4 (marked with *). However, the presence of small amount of Mn_3O_4 has little effect on the properties of MnO according to the results in Ref. [25], and the following activity tests can also confirm this deducing. Although the broad and weak diffraction lines in Fig. 1(d) demonstrate the bad crystallization, Au/MnO_2 can still be indexed to MnO_2 (JCPDS 012-0713). Moreover, the sharp diffraction peaks of Au, indicating the presence of large gold particles, are discerned on Au/MnO and Au/MnO_2 samples. Thus, according to the Scherrer equation, the average size of gold particles calculated from XRD patterns are 23.8 and 8.5 nm for Au/MnO and Au/MnO_2.

Table 1
The physico-chemical properties of Au/MnO_x catalysts.

Sample	S_{BET} (m^2/g)	Au[a] (wt.%)	d_{Au}[b] (nm)	D_{Au}[c] (nm)
MnO	10	–	–	–
MnO_2	52	–	–	–
Mn_2O_3	35	–	–	–
Au/MnO	8	5.5	3.1/26.2[d]	23.8
Au/MnO_2	39	5.3	3.0/11.5[d]	8.5
Au/Mn_2O_3	31	5.0	2.6	–
Used Au/Mn_2O_3[e]	33	5.3	2.7	–

[a] Determined by ICP-AES analysis with the error range of ±0.5%.
[b] Determined by TEM.
[c] Calculated by Scherrer equation from the XRD results.
[d] The average size of the small and the large gold particles.
[e] After being used for 4 times.

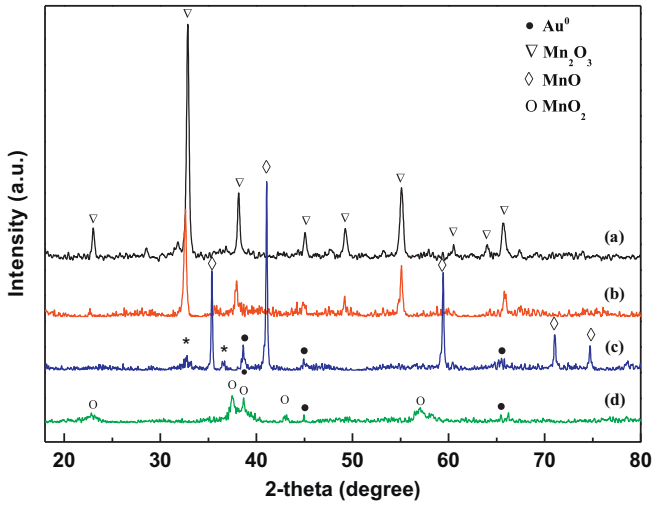

Fig. 1. XRD patterns of (a) Au/Mn_2O_3, (b) Au/Mn_2O_3 used for 4 times, (c) Au/MnO and (d) Au/MnO_2.

3.1.3. TEM results

Fig. 2 shows the Au particle-size distributions of the three kinds of catalysts. In Au/Mn_2O_3 (Fig. 2(e) and (f)), the images demonstrate that gold particles are in a narrow distribution and well dispersed with the average particle size of 2.6 nm. Clearly, the morphology of Au particles keeps intact after being used for 4 times (Fig. 2(g) and (h)). In contrast, the Au size distribution is relatively broad in Au/MnO (Fig. 2(a) and (b)) and Au/MnO_2 (Fig. 2(c) and (d)), suggesting a large heterogeneity of gold particles. Meanwhile, the two catalysts both display bimodal particle size distribution comprising two populations. For Au/MnO_2, the average gold sizes are 3.0 and 11.5 nm, while they are 3.1 and 26.2 nm in Au/MnO. The diversity of Au particle-size distribution may be related to the various phase structures and intrinsic properties of different supports (as discussed below). In the present work, the preparation method for the gold-based catalysts was the same (DP) and the results (the gold particle size and distribution) were the best under identical conditions.

The previous work has revealed that the applicability of urea DP method strongly depends on the nature of substrates, and it is beneficial to the deposition of gold onto oxide supports with point of zero charge (PZC) close to 6.0 [30,37]. According to the Zeta potential measurements, the PZC values for MnO, MnO_2 and Mn_2O_3 were estimated to be 7.3, 4.0 and 6.7, which are in agreement with the findings in literatures [39,40]. Therefore, this result well explains the presence of small and high dispersed gold nanoparticles obtained on the surface of Mn_2O_3.

3.1.4. XPS

Surface gold content and electronic state of the catalysts were characterized by XPS and the results are given in Table 2 and Figs. 3 and 4. In Au/MnO_2 (Fig. 3(a)), the Au 4f peak is quite symmetric and narrow, representing that there is only one kind of Au species (elemental state, 83.8 eV), or the amount of ionic gold is too small to be distinguished from the background. Broad peaks of Au 4f were observed in Au/MnO (Fig. 3(b)) and Au/Mn_2O_3 (Fig. 3(c)), indicating the possible presence of both metallic and ionic gold species [41,42]. Thus, the original peaks (broken line) of Au/MnO (Fig. 3(b)) and Au/Mn_2O_3 (Fig. 3(c)) were deconvolutioned into different peaks (solid line), and the binding energies of Au $4f_{7/2}$ peaks are 82.5 eV and 83.8 eV after the correction of charge effect. It is strange to find that the charge effect of binding energy in Au/MnO (5.4 eV, C 1s = 290.0 eV) and Au/Mn_2O_3 (5.4 eV, C 1s = 290.0 eV) is much bigger than that in Au/MnO_2 (0.6 eV, C 1s = 285.2 eV).

After the deconvolution of the Au 4f peaks, the binding energy difference in the two chemical states is 1.3 eV in Au/MnO and Au/Mn_2O_3 and an important component of Au is $Au^{\delta-}$, which means the formation of lots of anionic Au species with more than one charge ($\delta > 1$) if the charge effect was corrected by 5.4 eV. This finding is quite different from those reported in Au/MnO_x previously [30,31,45]. We think that the strange chemical shift of Au 4f may be an overcorrection of Au peaks by contaminant carbon in Au/MnO and Au/Mn_2O_3. Similar result has been also observed in the same XPS system on Ag/SiO_2 catalyst [43]. The two series of catalysts both have metals on the metal oxide support while the metals show different particle size or chemical states. Because the conductivity of metals is much better than the metal oxide supports, the charge effect many be different on the metals and the support. Moreover, there are always metallic and cationic Au species in the literatures [19–21,30–33] whose preparation methods or catalysts are similar to the present work. Thus, it is reasonable to believe that there are metallic and positively charged gold in our Au/MnO and Au/Mn_2O_3 catalysts. Detailed binding energies after the re-correction are listed in Table 2 in the parentheses. Under the same condition, due to the semiconductor character of MnO_2, the charge effect is very small and can be neglected. As a result, no anionic gold species was found on Au/MnO_2.

Combined with the above discussion, the support phase influences the electronic nature of gold particles and the proper content of $Au^{\delta+}$ suggests an appropriate gold–support interaction [20], and the amount of $Au^{\delta+}$ are 20% and 67% on the surface of Au/Mn_2O_3 and Au/MnO (after the reaction, the amount of $Au^{\delta+}$ increased from 20% to 57% in the used Au/Mn_2O_3 (Fig. 3(d))), indicating the proper metal–support interaction in Au/Mn_2O_3. Meanwhile, the previous investigations have found that Mn_2O_3 can promote the catalytic activity of gold catalyst better than other manganese oxides due to the intimate metal–support interaction, thus we believe the cationic gold is beneficial to the high activity, which is in well agreement with those reported earlier [28,44,45].

Mn 2p XPS spectra for various catalysts are shown in Fig. 4(a). The Au/MnO_2 catalyst exhibits an asymmetric Mn $2p_{3/2}$ peak located at 642.2 eV, which is in agreement with those reported in literature for MnO_2, i.e., 642.0 ± 0.2 eV [46]. It is found that the binding energies of Mn $2p_{3/2}$ shift to lower values in following order: $Au/MnO_2 > Au/Mn_2O_3 > Au/MnO$, and they are all close to the values of pure supports. Nevertheless, the variation of XPS binding energies of Mn 2p alone is too small to precisely evaluate the Mn valence of MnO_x [47]. Therefore, the corresponding Mn 3s spectra were measured simultaneously (Mn 3s ΔE) to estimate the Mn chemical states. Yet the Au 4f doublet overlaps with the Mn 3s multiplet splitting peaks, so we constrained the relative position and intensity of Mn 3s components by assuming for the gold-containing samples the same Mn 3s/Mn 2p intensity ratio as for the bare supports [48] and the curve fitting results are listed in Table 2. It is shown that the values of Mn 3s ΔE before and after Au dispersion are nearly invariable, suggesting the Mn chemical states are little effected by the deposition of gold particles. Comparing with the literatures, the values of the Mn 3s ΔE does not decrease monotonically with the increase of nominal valence of MnO_x, this is attributed to the difference of preparation methods and test conditions. It is interesting to find that the Mn 3s ΔE values of MnO and Mn_2O_3 both are lower than that in Ref. [47], but they present the same decreasing trend as that in the reference. Because of the very different synthesis process, the Mn 3s ΔE value in MnO_2 is higher than that in Ref. [47]. However, the Mn 3s ΔE value of MnO_2 is in agreement with the results observed by Longo et al. [48], whose preparation method and crystal phase of MnO_2 are similar to the present work.

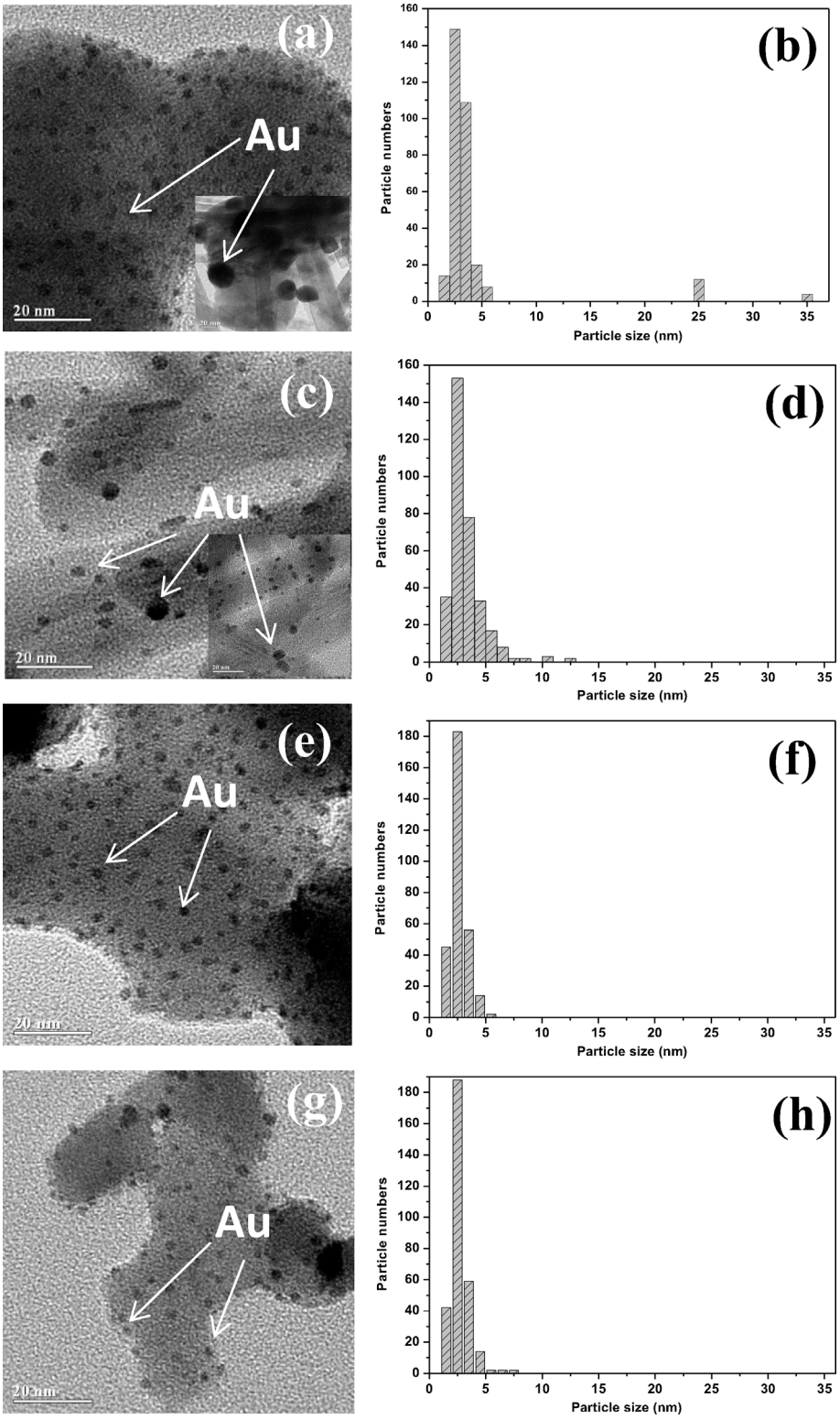

Fig. 2. TEM images and particle size distributions of Au/MnO (a, b), Au/MnO_2 (c, d), Au/Mn_2O_3 (e, f), and Au/Mn_2O_3 used for 4 times (g, h).

The O 1s spectra of various Au/MnO_x are also presented in Fig. 4(b). The main peak at about 529.0 eV is attributed to the lattice oxygen bonded to Mn atoms [49]. Simultaneously, distinct shoulders, which can be assigned to the mixture of hydroxyl groups and adsorbed water on the surface of catalysts [50], are visible on the higher binding energy side of the main peaks. It is found that the Au/MnO catalyst has the highest surface molar ratio of gold to Mn (Au/Mn, 0.50), which may be a result of the lowest BET of MnO support. The Au/Mn ratio is 0.48 in Au/Mn_2O_3, which is much higher than that in Au/MnO_2 (0.27). The relatively lower Au/Mn value in Au/MnO_2 sample is due to the highly acidic nature of MnO_2 [30], and Mn_2O_3 can facilitate the dispersion of gold on the surface of

Table 2
XPS results of Au/MnO_x catalysts.

Sample	BE of Au 4f 7/2 (eV)[c]	Au species (%)	BE of Mn 2p 3/2 (eV)	Mn 3s ΔE	Au/Mn	O_T/Mn[a]	O_L/Mn[b]
MnO	–	–	641.8	5.5	–	2.08	1.01
Au/MnO	82.5 (83.8) 83.8 (85.1)	Au^0 (33) $Au^{\delta+}$ (67)	641.7	5.3	0.50	1.99	0.98
MnO_2	–	–	642.3	5.4	–	2.52	1.33
Au/MnO_2	83.8	Au^0 (100)	642.2	5.4	0.27	2.56	1.35
Mn_2O_3	–	–	642.1	4.6	–	2.43	0.95
Au/Mn_2O_3	82.5 (83.8) 83.8 (85.1)	Au^0 (80) $Au^{\delta+}$ (20)	641.9	4.6	0.48	2.37	0.93
Used Au/Mn_2O_3	82.5 (83.8) 83.8 (85.1)	Au^0 (43) $Au^{\delta+}$ (57)	641.9	4.6	0.48	2.67	0.99

[a] O_T, total surface oxygen.
[b] O_L, surface lattice oxygen.
[c] Data in the parentheses, charge effect was corrected by 4.1 eV.

support [30]. After being used for 4 times, no variation of Au/Mn ratio is found in Au/Mn_2O_3, suggesting this catalyst has superior stability.

Furthermore, the molar ratios of the total amount of surface oxygen (O_T) to Mn were calculated and these values are much higher than the stoichiometric ones, indicating the presence of a high concentration of oxygen-containing adsorbates on the surface of catalysts [30,50]. The peak deconvolution of the O 1s lines gives more information about the relative amount of different surface oxygen species. As shown in Table 2, the molar ratios of surface lattice oxygen (O_L, 529.0 eV) to Mn are 0.93, 0.98 and 1.35 in Au/Mn_2O_3, Au/MnO, and Au/MnO_2, respectively. They are all less than the stoichiometric values (1.5, 1.0 and 2.0 in Au/Mn_2O_3, Au/MnO, and Au/MnO_2), inferring the emerging of surface oxygen vacancies which are filled with water or hydroxyl groups. It is clear that the Au/Mn_2O_3 catalyst owns the maximum oxygen vacancies because of the minimum O_L/Mn ratio (0.93) that is less than the stoichiometric value (1.5). The surface oxygen vacancies are considered as a key role in promoting the catalytic activity by enhancing the electron transfer between the support and gold particles and can be regenerated under reaction conditions [48,51–54]. After four times reaction over Au/Mn_2O_3, the

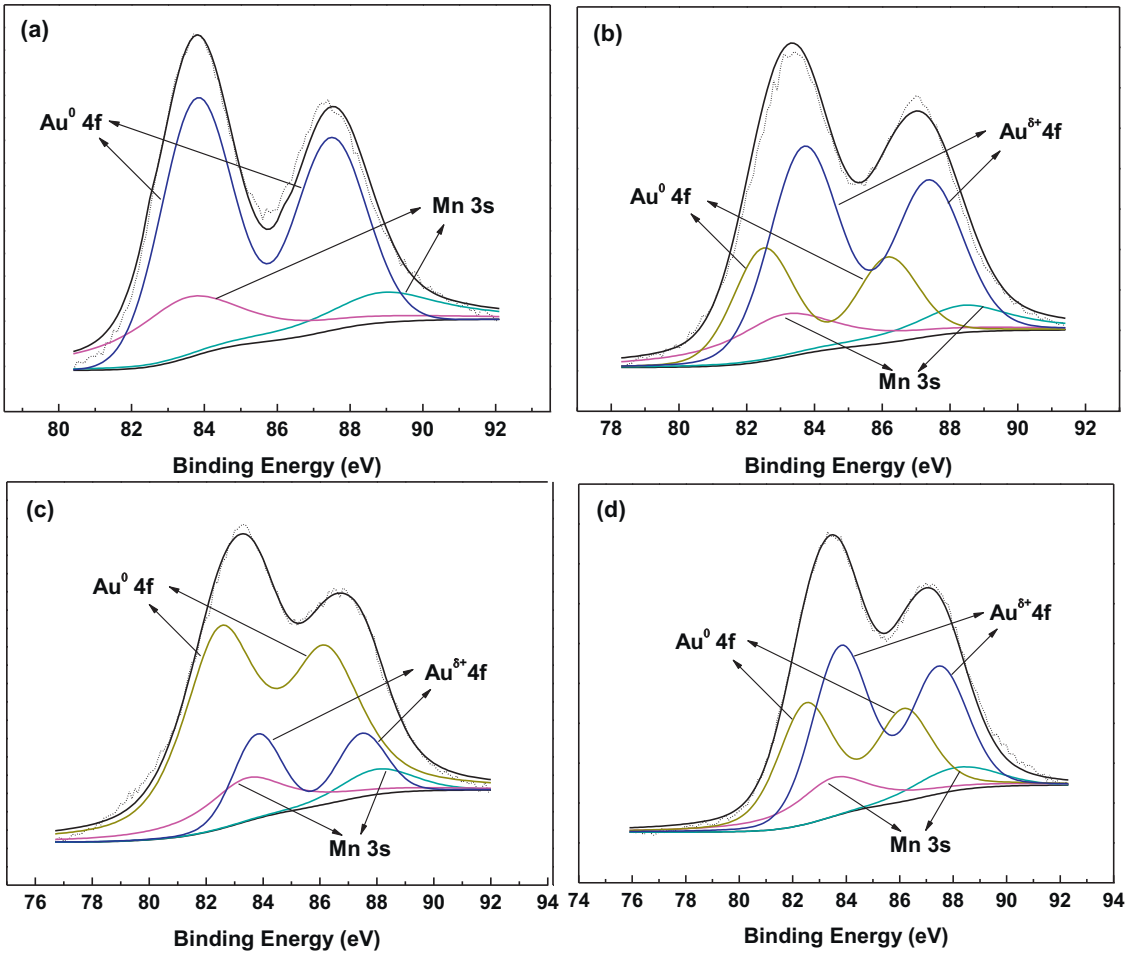

Fig. 3. Mn 3s and Au 4f XPS spectra of (a) Au/MnO_2, (b) Au/MnO, (c) Au/Mn_2O_3, and (d) Au/Mn_2O_3 used for 4 times.

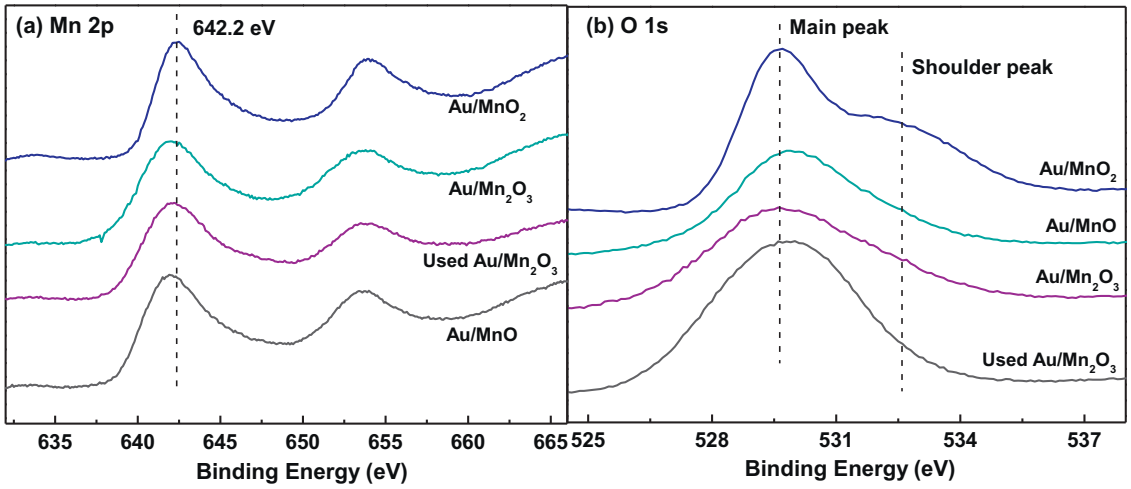

Fig. 4. (a) Mn 2p XPS spectra of Au/MnO_2, Au/Mn_2O_3, Au/Mn_2O_3 used for 4 times and Au/MnO. (b) O 1s XPS spectra of Au/MnO_2, Au/MnO, Au/Mn_2O_3 and Au/Mn_2O_3 used for 4 times.

O_T/Mn and O_L/Mn ratios increased slightly, revealing the oxygen vacancies relatively decreased, and it also implies that the oxygen vacancies participated in the oxidation reaction process and the produced oxygen-containing group would occupy the oxygen vacancies during the reaction. Thus, the oxygen vacancies are supposed to facilitate the reaction. In addition, the O_T/Mn and O_L/Mn ratios could be recovered after the activation of the used catalyst with air at 573 K.

3.2. Catalytic oxidative lactonization of 1,4-butanediol

The catalytic results of Au/MnO_x in the oxidative lactonazation of 1,4-butanediol to γ-butyrolactone are given in Table 3 and Fig. 5. For comparison, activities of bare carriers are also included. Obviously, the pure supports hardly catalyzed the reaction, but the catalytic activities were distinctly improved after the deposition of gold. All the three catalysts exhibit excellent selectivity of 100%, which can greatly facilitate the process of product separation after the reaction, and the Au/Mn_2O_3 catalyst displays a prominent activity with 4-h-conversion of 91%. After 8 h reaction, the conversions are 98%, 75% and 50% for Au/Mn_2O_3, Au/MnO_2, Au/MnO. Besides, we tested a catalyst with gold deposited on pure Mn_3O_4, whose catalytic activity was similar to that of Au/MnO_2. Thus, we suppose that the small amount of Mn_3O_4 would not lower the activity of Au/MnO at least. However, there is a little surprising for Au/MnO_2 and Au/MnO. Considering the relatively large gold particles estimated from XRD patterns and TEM images, both of them expressed admirable activities.

For evaluating the catalytic ability, we estimated the TON values for all the gold-supported catalysts. The TON value of Au/Mn_2O_3

Table 3
Catalytic activity of Au/MnO_x catalysts in the oxidative lactonization of 1,4-butanediol.[a]

Sample	Conversion (%)	Yield (%)	TOF[b] (h^{-1})	TON[c]
MnO	1	1	–	–
MnO_2	2	2	–	–
Mn_2O_3	5	5	–	–
Au/MnO	50	50	473	142
Au/MnO_2	75	75	728	193
Au/Mn_2O_3	98	98	1352	261
Au/Mn_2O_3[d]	95	95	1341	253

[a] Reaction conditions: 0.3 g catalyst, 1.4 g 1,4-butanediol, 20 ml TBP, 1.25 MPa air, 393 K, 8 h.
[b] TOF value was calculated as mol 1,4-butanediol reacted in the initial 2 h on per mol surface gold calculated from the gold dispersion by TEM.
[c] TON value was calculated as the amount of 1,4-butanediol reacted per mole gold.
[d] The catalyst was preserved for one year.

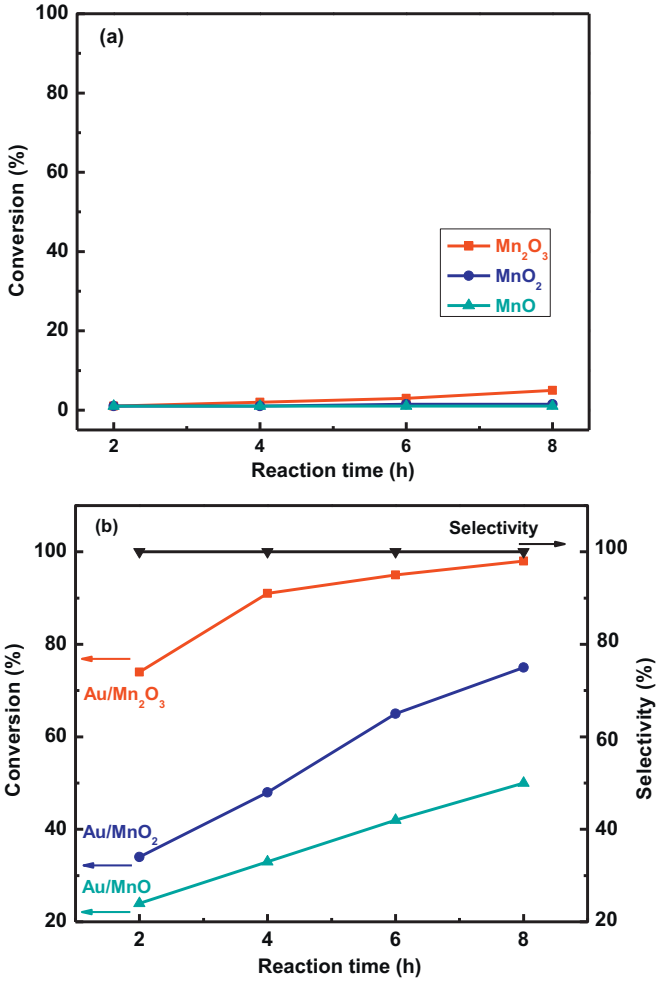

Fig. 5. Time course of the oxidative lactonization of 1,4-butanediol catalyzed by parent MnO_x (a) and Au/MnO_x (b). Reaction conditions: 0.3 g catalyst, 1.4 g 1,4-butanediol, 20 ml TBP, 1.25 MPa air, 393 K.

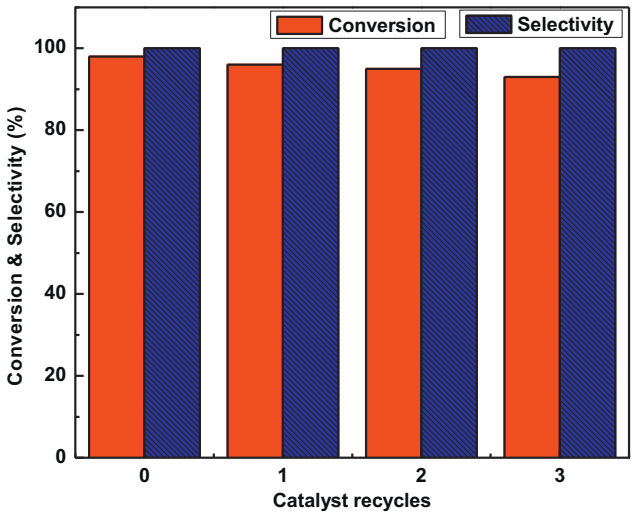

Fig. 6. Recyclability of the oxidative lactonization of 1,4-butanediol catalyzed by Au/Mn_2O_3 catalyst. Reaction conditions: 0.3 g catalyst, 1.4 g 1,4-butanediol, 20 ml TBP, 1.25 MPa air, 393 K.

is 261, which is much inferior to the ruthenium complexes (TON: 3170-17000) [11] and Au/hydrotalcite (TON: 1400) [12]. It is known that the ruthenium complexes are homogeneous which can make a good contact with the reactant and there is strong anion-exchange ability in hydrotalcite, which can both greatly facilitate the reaction. However, compared with other reducible oxide supported gold catalysts: Au/TiO_2 (TON: 101) [19], and Au/FeO_x (TON: 300) [20], the TON value of Au/Mn_2O_3 is comparable to those reported earlier. Additionally, the TOF values were also calculated, and they are 1352, 728 and 473 h^{-1} for Au/Mn_2O_3, Au/MnO_2 and Au/MnO, respectively. To our knowledge, the first two values are much greater than that in Au/TiO_2 (64 h^{-1}) [19] and Au/FeO_x (624 h^{-1}) [20]. Especially, the Au/Mn_2O_3 showed at least 2 times higher activity than Au/FeO_x, which can be considered as a promising candidate in the lactonization of 1,4-butanediol.

Recycling experiments were also conducted over Au/Mn_2O_3. The sample was used for 4 successive reactions without apparent loss of catalytic activity as shown in Fig. 6. Moreover, we have tested a Au/Mn_2O_3 catalyst that was preserved in glass desiccators without any special protection for more than one year. To our great surprise, this catalyst also showed analogous great catalytic activity (95%), which alters the traditional impression that gold catalyst is always hard to be stored and to keep its initial catalytic performances for a long period of time [55,56]. Additionally, we operated the leaching test by ICP-AES analysis, there was no leaching of Au or Mn being detected in the reaction mixture, indicating the special stability of Au/Mn_2O_3.

Furthermore, the Au/Mn_2O_3 catalyst was also used in the lactonizations of a series of α,ω-diols to afford corresponding lactones, including 1,2-benzenedimethanol, 1,5-pentanediol and 1,6-hexanediol, and the corresponding catalytic activities are listed in Table 4. It is found that their selectivities are all above 90%, but the conversions are 50%, 48% and 10%, respectively. These values are much lower than that in 1,4-butanediol, due to the shorter carbon chain and smaller steric hindrance of cyclization in 1,4-butanediol molecule. Meanwhile, γ-butyrolactone is a very stable lactone with five-membered ring, which is beneficial to the reaction.

Table 4
Catalytic activity of Au/Mn_2O_3 catalyst in the oxidative lactonization of α,ω-diols.[a]

Diol	Conversion (%)	Selectivity (%)	Yield (%)
1,4-Butanediol	98	100	98
1,5-Pentanediol	48	90	43
1,6-Hexanediol	10	90	9
1,2-Benzenedimethanol	50	96	48

[a] Reaction conditions: 16 mmol α,ω-diols, Au/diol = 1/200, 20 ml TBP, 1.25 MPa air, 393 K, 8 h.

4. Conclusions

We have demonstrated that Au/MnO_x catalysts prepared by urea DP method were very active for the aerobic lactonization of 1,4-butanediol to γ-butyrolactone with air as the oxidant. These catalysts showed selectivity of 100% that could simplify the separation of the products after the reaction. The highest conversion of 98% was achieved by using Au/Mn_2O_3 after 8 h reaction. Compared with other Au/MnO_x catalysts, we believed that the superior activity of Au/Mn_2O_3 could be attributed to the presence of highly dispersed gold particles and the intrinsic properties of Mn_2O_3, including the appropriate point of zero charge for DP method, the most quantity oxygen vacancies and the formation of the appropriate metal–support interaction. Moreover, the Au/Mn_2O_3 catalyst could be recycled by simple treatment and kept for a long time without losing any catalytic activity. However, studies on the intrinsic nature of Au/MnO_x by using Mn_2O_3 with different gold particle size and different manganese oxides with the same sized gold particles are being under way.

Acknowledgements

This work was financially supported by the Major State Basic Resource Development Program (Grant No. 2012CB224804), NNSFC (Project 20903035, 20973042, 21173052), and the Natural Science Foundation of Shanghai Science and Technology Committee (08DZ2270500). The authors sincerely thank the reviewers for their useful suggestions on the chemical state analysis of Au/MnO_x.

References

[1] Y. Sasaki, Electrochemistry 76 (2008) 161–164.
[2] A.C. Albertsson, I.K. Varma, Biomacromolecules 4 (2003) 1466–1486.
[3] S. Kobayashi, Macromol. Symp. 240 (2006) 178–185.
[4] H. Lee, F.Q. Zeng, M. Dunne, C. Allen, Biomacromolecules 6 (2005) 3119–3128.
[5] M. Fetizon, M. Golfier, J.M. Louis, Chem. Commun. (1969) 1118–1119.
[6] P. Johnton, R.C. Sheppard, C.E. Stehr, S. Turner, J. Chem. Soc. C (1966) 1847–1856.
[7] T. Suzuki, K. Morita, M. Tsuchida, K. Hiroi, Org. Lett. 4 (2002) 2361–2363.
[8] M. Ito, A. Osaku, A. Shiibashi, T. Ikariya, Org. Lett. 9 (2007) 1821–1824.
[9] K. Hari Prasad Reddy, N. Anand, P.S. Sai Prasad, K.S. Rama Rao, B. Dacid Raju, Catal. Commun. 12 (2011) 866–869.
[10] W.B. Hou, N.A. Dehm, R.W.J. Scott, J. Catal. 253 (2008) 22–27.
[11] J. Zhao, J.F. Hartwig, Organometallics 24 (2005) 2441–2446.
[12] T. Mitsudome, A. Noujima, T. Mizugaki, K. Jitsukawa, K. Kaneda, Green Chem. 11 (2009) 793–797.
[13] J. Huang, Y. Wang, J.M. Zheng, W.L. Dai, K.N. Fan, Appl. Catal. B: Environ. 103 (2011) 343–350.
[14] W. Oberhauser, A. Lavacchi, F. Vizza, L. Capozzoli, Appl. Catal. A: Gen. 451 (2013) 58–64.
[15] A.S.K. Hashmi, G.J. Hutchings, Angew. Chem. Int. Ed. 45 (2006) 7896–7936.
[16] B.K. Min, C.M. Friend, Chem. Rev. 107 (2007) 2709–2724.
[17] M.M. Schubert, S. Hackenberg, A.C. van Veen, M. Muhler, V. Plzak, R.J. Behm, J. Catal. 197 (2001) 113–122.
[18] S. Carrettin, P. Concepción, A. Corma, J.M. Lopez Nieto, V.F. Puntes, Angew. Chem. Int. Ed. 43 (2004) 2538–2540.
[19] J. Huang, W.L. Dai, H.X. Li, K.N. Fan, J. Catal. 252 (2007) 69–76.
[20] J. Huang, W.L. Dai, K.N. Fan, J. Phys. Chem. C 112 (2008) 16110–16117.
[21] J. Huang, W.L. Dai, K.N. Fan, J. Catal. 266 (2009) 228–235.
[22] J.M. Zheng, J. Huang, X. Li, W.L. Dai, K.N. Fan, RSC Adv. 2 (2012) 3801–3809.
[23] F. Wang, G. Yang, W. Zhang, W. Wu, J. Xu, Adv. Synth. Catal. 346 (2004) 633–638.
[24] V.R. Choudhary, J.R. Indurkar, V.S. Narkhede, R. Jha, J. Catal. 227 (2004) 257–261.
[25] X.Q. Li, J. Xu, F. Wang, J. Gao, L.P. Zhou, G.Y. Yang, Catal. Lett. 108 (2006) 137–140.
[26] Y. Su, L.C. Wang, Y.M. Liu, Y. Cao, H.Y. He, K.N. Fan, Catal. Commun. 8 (2007) 2181–2185.
[27] T. Ishida, H. Watanabe, T. Takei, A. Hamasaki, M. Tokunaga, M. Haruta, Appl. Catal. A: Gen. 425–426 (2012) 85–89.
[28] L.M. Martinez.T, F. Romero-Sarria, W.Y. Hernandez, M.A. Centeno, J.A. Odriozola, Appl. Catal. A: Gen. 423–424 (2012) 137–145.

[29] Q. Ye, J.S. Zhao, F.F. Huo, D. Wang, S.Y. Cheng, T.F. Kang, H.X. Dai, Microporous Mesoporous Mater. 172 (2013) 20–29.
[30] L.C. Wang, Q. Liu, X.S. Huang, Y.M. Liu, Y. Cao, K.N. Fan, Appl. Catal. B: Environ. 88 (2009) 204–212.
[31] L.C. Wang, L. He, Y.M. Liu, Y. Cao, H.Y. He, K.N. Fan, J.H. Zhuang, J. Catal. 264 (2009) 145–153.
[32] L.C. Wang, Y.M. Liu, M. Chen, Y. Cao, H.Y. He, K.N. Fan, J. Phys. Chem. C 112 (2008) 6981–6987.
[33] L.C. Wang, L. He, Q. Liu, Y.M. Liu, M. Chen, Y. Cao, H.Y. He, K.N. Fan, Appl. Catal. A: Gen. 344 (2008) 150–157.
[34] G.C. Bond, C. Louis, D.T. Thompson, in: G.J. Hutchings (Ed.), Catalysis by Gold, Catalytic Science Series, vol. 6, Imperial College Press, London, 2006.
[35] X.Y. Deng, B.K. Min, A. Guloy, C.M. Friend, J. Am. Chem. Soc. 127 (2005) 9267–9270.
[36] R. Zanella, S. Giorgio, C.R. Henry, C. Louis, J. Phys. Chem. B 106 (2002) 7634–7642.
[37] R. Zanella, S. Giorgio, C.H. Shin, C.R. Henry, C. Louis, J. Catal. 222 (2004) 357–367.
[38] J. Radnik, L. Wilde, M. Schneider, M.M. Pohl, D. Herein, J. Phys. Chem. B 110 (2006) 23688–23693.
[39] M. Kosmulski, J. Colloid Interface Sci. 253 (2002) 77–87.
[40] P.S. Nico, R.J. Zasoski, Environ. Sci. Technol. 34 (2006) 3363–3367.
[41] S.D. Gardner, G.B. Hoflund, M.R. Davidson, H.A. Laitinen, D.R. Schryer, B.T. Upchurch, Langmuir 7 (1991) 2140–2145.
[42] R. Leppelt, B. Schumacher, V. Plzak, M. Kinne, R.J. Behm, J. Catal. 244 (2006) 137–152.
[43] Y. Cao, W.L. Dai, J.F. Deng, Appl. Catal. A: Gen. 158 (1997) 27–34.
[44] H. Trevino, G.D. Lei, W.M.H. Sachtler, J. Catal. 154 (1995) 245–252.
[45] L.C. Wang, X.S. Huang, Q. Liu, Y.M. Liu, Y. Cao, H.Y. He, K.N. Fan, J.H. Zhuang, J. Catal. 259 (2008) 66–74.
[46] F. Kapteijn, A.D. van Langeveld, J.A. Mpulijin, A. Andreini, M.A. Vuurman, A.M. Turek, J.M. Jehng, I.E. Wachs, J. Catal. 150 (1994) 94–104.
[47] Y.F. Han, F.X. Chen, Z.Y. Zhong, K. Ramesh, L.W. Chen, E. Widjaja, J. Phys. Chem. B 110 (2006) 24450–24456.
[48] A. Longo, L.F. Liotta, G.D. Carlo, F. Giannici, A.M. Venezia, A. Martorana, Chem. Mater. 22 (2010) 3952–3960.
[49] S.D. Gardner, G.B. Hoflund, M.R. Davidson, D.R. Schryer, J. Schryer, B.T. Upchurch, E.J. Kielin, Langmuir 7 (1991) 2135–2140.
[50] S.J. Lee, A. Gavriilidis, Q.A. Pankhurst, A. Kyek, F.E. Wagner, P.C.L. Wong, K.L. Yeung, J. Catal. 200 (2001) 298–308.
[51] J.A. Rodriguez, G. Liu, T. Jirsak, J. Hrek, Z. Chang, J. Dvorak, A. Maiti, J. Am. Chem. Soc. 124 (2002) 5242–5250.
[52] A.K. Sinha, K. Suzuki, M. Takanara, H. Azuma, T. Nonaka, K. Fukumoto, Angew. Chem. Int. Ed. 46 (2007) 2891–2894.
[53] A.K. Sinha, K. Suzuki, M. Takahara, H. Azuma, T. Nonaka, N. Suzuki, N. Takahashi, J. Phys. Chem. C 112 (2008) 16028–16035.
[54] D. Andreeva, I. Ivanov, L. Ilieva, J.W. Sobczak, G. Avdeev, K. Petrov, Top. Catal. 44 (2007) 173–182.
[55] R. Zanella, C. Louis, Catal. Today 768 (2005) 107–108.
[56] G.F. Zhao, M. Ling, H.Y. Hu, M.M. Deng, Q.S. Xue, Y. Lu, Green Chem. 13 (2001) 3088–3092.